

# Phase diagrams, critical and multicritical behavior of hard-core Bose-Hubbard models

Christian Pich<sup>a</sup> and Erwin Frey<sup>b</sup>

<sup>a</sup>*Physics Department, University of California, Santa Cruz, CA 95064*

<sup>b</sup>*Institut für Theoretische Physik, Technische Universität München, D-85747 Garching, Germany*

(March 24, 2022)

We determine the zero-temperature phase diagram of the hard-core Bose-Hubbard model on a square lattice by mean-field theory supplemented by a linear spin-wave analysis. Due to the interplay between nearest and next-nearest neighbor interaction and cubic anisotropy several supersolid phases with checkerboard, stripe domain or intermediate symmetry are stabilized. The phase diagrams show three different topologies depending on the relative strength of nearest and next-nearest neighbor interaction. We also find a rich variety of new quantum critical behavior and multicritical points and discuss the corresponding effective actions and universality classes.

PACS numbers: 67.40.Db, 05.30.Jp, 67.90 + z

## I. INTRODUCTION

Since the original suggestion by Andreev and Lifshitz [1], Chester [2] and Leggett [3] that quantum crystals such as <sup>4</sup>He might exhibit a phase where superfluidity coexists with crystalline order the topic of supersolids has received considerable theoretical attention. Early theoretical work (for a review see e.g. Ref. [4]) focused on the possible implications of large zero-point vibrations in establishing a supersolid phase in quantum crystals. It was argued by Andreev and Lifshitz [1] that these quantum effects might be sufficient to delocalize either impurities and/or zero-point vacancies. Such a system would form a weakly interacting Bose gas and therefore be a beautiful example of a system which shows Bose-Einstein condensation. Upon exploiting a mapping between hard-core lattice gas models and spin-1/2 Heisenberg models it was shown that within a mean-field approximation such a supersolid phase exists for systems with a finite range of interactions between the bosons [5,6].

Unfortunately, there is not yet clear experimental evidence for such a phase. The most promising candidates for experimental systems, where supersolid order might be observed, are Josephson junction arrays and <sup>4</sup>He films on substrates in two dimensions. There have also been experimental searches for supersolid order in bulk <sup>4</sup>He. In ultrasound studies [7] of highly purified solid <sup>4</sup>He a recently observed resonance phenomenon was interpreted to be consistent with the presence of a supersolid induced by zero-point vacancies. But the experimental situation still remains controversial [8], and additional evidence is needed to unambiguously prove the existence of such a phase. Artificially fabricated Josephson junction arrays are a particular interesting system for the observation of exotic phases in quantum systems. Finite-range interactions and frustrations present in these arrays give rise to a rather rich structure of the phase diagram.

Partly motivated by this controversial experimental situation, recent work has concentrated on mapping out

the phase diagram of strong interacting clean bosonic systems mainly through numerical and mean-field approximation [9–14]. The starting point of these investigations are lattice models of interacting bosons with the following Bose-Hubbard Hamiltonian,

$$\mathcal{H} = -\frac{t}{2} \sum_{\langle i,j \rangle} (a_i^\dagger a_j + a_j^\dagger a_i) - \mu \sum_i n_i + \sum_{i,j} n_i U_{ij} n_j. \quad (1.1)$$

Here  $a_i$ ,  $a_i^\dagger$  are boson annihilation and creation operators at site  $i$ , and  $n_i = a_i^\dagger a_i$ . The hopping integral  $t$  sets the energy scale,  $\mu$  is the chemical potential, and  $U_{ij}$  denotes the interaction between the bosons. Bosons only hop to adjacent places ( $\langle i,j \rangle$ ). It is found that for nearest neighbor interaction supersolid order at half-filling is favored at large nearest neighbor interaction  $U_1$  and small on-site interaction  $U_{ii} = U_0$ , but becomes suppressed in the hard-core limit [14]. In the latter case next-nearest neighbor interactions become necessary for supersolid order to exist [6]. Besides the quantum ground states at half filling, which may be either a checkerboard or stripe domain density wave, additional Mott-insulating phases with a density wave commensurate with the underlying lattice appear. Each of these phases seems to have an associated supersolid phase in which the particular charge-density order coexists with off-diagonal long range order. As we will show here, however, there are intermediate supersolid phases which have no Mott-insulating partner in the phase diagram.

In the present work we report on a mean-field analysis of the hard-core next-nearest neighbor Bose-Hubbard model supplemented by a linear spin-wave analysis. Our purpose is to map out the phase diagram over the whole range of parameters of nearest and next-nearest interaction. This extends previous work by Bruder et al. [9], which has been restricted to a small value of the next-nearest neighbor interaction, where the ground state possesses checkerboard symmetry. Furthermore, we determine the order and universality class of the phase transi-

tions and identify various interesting multicritical points.

We focus on strong on-site interaction  $U_{ii} = U_0$ , i.e. a hard-core approximation where the particle number per site takes only values between the integer values  $n$  and  $n+1$  (in the vicinity of half-filling). Then the model can be transformed in a spin-1/2 XXZ model [5]

$$\begin{aligned} \mathcal{H} = & -J \sum_{\langle i,j \rangle} (S_i^x S_j^x + S_i^y S_j^y) + U_1 \sum_{\langle i,j \rangle} S_i^z S_j^z \\ & + U_2 \sum_{\langle\langle i,j \rangle\rangle} S_i^z S_j^z - h \sum_i S_i^z, \end{aligned} \quad (1.2)$$

where we have dropped a constant energy offset. The mapping is performed by identifying  $a_i^\dagger = S_i^x + iS_i^y$ ,  $n_i = S_i^z + \frac{1}{2}$ ,  $J = t$  and  $h = \mu - \sum_i U_{0i}$ . Here  $\langle i, j \rangle$  denotes the nearest neighbors and  $\langle\langle i, j \rangle\rangle$  the next-nearest neighbors. After a Fourier transform,  $S_i^\alpha = \frac{1}{\sqrt{N}} \sum_q e^{iqx_i} S_q^\alpha$ , the Hamiltonian can be written as

$$\begin{aligned} \mathcal{H} = & - \sum_q \left[ J_q (S_q^x S_{-q}^x + S_q^y S_{-q}^y) \right. \\ & \left. + (U_{1q} + U_{2q}) S_q^z S_{-q}^z \right] - \sqrt{N} h S_{q=0}^z \end{aligned} \quad (1.3)$$

with the interaction terms

$$J_q = z_1 J \gamma_q, \quad (1.4a)$$

$$U_{1q} = -z_1 U_1 \gamma_q, \quad (1.4b)$$

$$U_{2q} = -z_2 U_2 \eta_q. \quad (1.4c)$$

The structure factors

$$\gamma_q = \frac{1}{z_1} \sum_{l \in \text{n.n.}} e^{iqx_l}, \quad \text{and} \quad \eta_q = \frac{1}{z_2} \sum_{l \in \text{n.n.n.}} e^{iqx_l} \quad (1.5)$$

depend on the lattice structure and are defined as sums over the nearest neighbor sites  $z_1$  and next-nearest neighbor sites  $z_2$ , respectively.

In this paper we use classical ground state analysis and linear spin-wave theory to explore the phase diagram of the hard-core Bose-Hubbard system with nearest and next-nearest neighbor “charge”-interaction,  $U_{ij}$ , and a nearest neighbor hopping term,  $J$ . We focus our study on the bipartite square lattice. For a discussion of frustrated two-dimensional lattices, like the triangular and Kagomé lattice, we refer the reader to a recent paper by Murthy et al. [15].

Linear spin-wave theory is implemented in its standard form. First, one calculates the classical ground state energy and the corresponding spin configuration, which frequently may be described by some ordering wave vector  $\tilde{q}$ . Next, local rotations of the spins are performed,  $S_i^\alpha \rightarrow \tilde{S}_i^\alpha$ , such that the  $z$ -component  $\tilde{S}_i^z$  points along the direction of the classical spin configuration. Upon performing a Holstein-Primakoff transformation, which in Fourier space is given by (for those ground states which can be described by a single wave vector  $\tilde{q}$ )

$$\tilde{S}_q^x = \sqrt{\frac{S}{2}} (a_{-q} + a_q^\dagger), \quad (1.6a)$$

$$\tilde{S}_q^y = -i\sqrt{\frac{S}{2}} (a_{-q-\tilde{q}} - a_{q+\tilde{q}}^\dagger), \quad (1.6b)$$

$$\tilde{S}_q^z = \sqrt{N} S \delta_{q,\tilde{q}} - \frac{1}{\sqrt{N}} \sum_p a_{p-q-\tilde{q}}^\dagger a_p, \quad (1.6c)$$

a linearized spin-wave Hamiltonian  $\mathcal{H}_{\text{sw}}$ , describing the elementary excitation around the classical ground state, is obtained.

The outline of the paper is as follows. In section II we study the phase diagram of the hard-core Bose-Hubbard model with nearest and next-nearest neighbor interaction. The analysis is done by employing the mapping to the spin-1/2 XXZ model and using a mean-field analysis supplemented by a linear spin-wave analysis. This allows us to determine the ground state spin configurations in the spin-1/2 XXZ model and analyze its stability and soft-modes by linear spin-wave theory. The resulting phase diagrams are given in section III together with a discussion of the universality classes of the critical phenomena at the various phase boundaries. We also identify a series of multicritical points and discuss their multicritical behavior. Our results and conclusions are given in section IV. Finally, some technical details about the linear spin-wave analysis of the Mott insulating 3/4 phase and the checkerboard and stripe domain supersolid phases are deferred to the appendices.

## II. MEAN-FIELD AND LINEAR SPIN-WAVE THEORY

In this section we analyze the phase diagram of the next-nearest neighbor hard-core Bose-Hubbard model, using a mean-field analysis supplemented by a linear spin-wave analysis. However, before discussing the effect of next-nearest neighbor interactions let us shortly summarize the topology of the phase diagram when the interaction  $U_{ij}$  is restricted to nearest neighbors. The phase diagram of the spin-1/2 XXZ Heisenberg model becomes particularly simple [9] (s. Fig. 1). There is a “half-integer” lobe (Néel phase) centered around zero magnetic field ( $J < U_1$ ). In the original Bose-Hubbard model this corresponds to the half-filling Mott-insulating phase with a checkerboard charge density wave. For increasing magnetic field (away from half-filling) this phase becomes unstable to a canted ferromagnetic state, i.e. the corresponding bosonic system becomes superfluid. Finally, for strong fields the system goes into a paramagnetic state with magnetization pointing in the field direction. Such a state has uniform density of bosons and is insulating again.

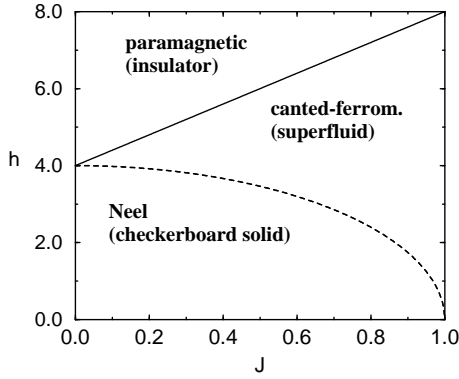


FIG. 1. Mean-field phase diagram of a two-dimensional hard-core Bose-Hubbard with nearest neighbor interaction  $U_1 = 1$  and  $S = 1/2$ . The Néel, canted-ferromagnetic and paramagnetic phase in the spin-1/2 XXZ model correspond to a Mott insulating phase with a checkerboard charge ordering, superfluid and a insulating phase with a homogeneous charge density, respectively. Second and first order phase transitions are indicated by solid and dashed lines, respectively.

Taking into account longer-range interactions, the phase diagram acquires further structure. In addition to the phases discussed above, one finds more general insulating phases and superconducting phases in which the spins arrange in a  $2 \times 2$  unit cell. In particular one can identify regions in parameter space where coexistence of long-range order in the  $xy$ -direction and staggered magnetization in the  $z$ -direction appear. This implies that the corresponding bosonic system would be a supersolid, since there is coexistence of crystalline order and superfluidity. A recent analysis of the classical ground state energies by Bruder et al. [9] identifies two different supersolid phases, which are characterized by two or three angles in the  $2 \times 2$  unit cell. However, their analysis has been restricted to small values of the next-nearest neighbor interaction, where the ground state possesses checkerboard symmetry. Here we extend the mean-field analysis of Ref. [9] to the full range of the parameters, where the ground state of the Bose-Hubbard model at half-filling possesses stripe symmetry. In addition we supplement the analysis of the classical ground state energy by a linear spin-wave analysis. In performing a spin-wave analysis we can check whether the ground state found by energy considerations is stable. In general, one has to minimize within a small symmetry class (an Ansatz), i.e. we make an Ansatz for the number of sublattices we need. From stability investigations we can confirm the ground state analysis, and we can evaluate the boundaries to the adjacent phases which occur as a soft-mode. In addition, the wave vector of the soft-mode gives a hint of the adjacent phase structure. Moreover, we obtain the contribution of the quantum fluctuations to the reduction of the true ground state energy and the order parameter.

Now we turn to a linear spin-wave analysis of the model, taking into account next-nearest neighbor inter-

action. For that we need the wave vector dependence of the interaction parameters in the linear spin-wave Hamiltonian. On a square lattice ( $xy$ -plane) there are four nearest and four next-nearest neighbors ( $z_1 = z_2 = 4$ ) and the structure factors are given by ( $a = 1$ )

$$\gamma_q = \frac{1}{2}(\cos q_x + \cos q_y), \quad (2.1)$$

$$\eta_q = \frac{1}{2}(\cos(q_x + q_y) + \cos(q_x - q_y)) = \cos q_x \cos q_y. \quad (2.2)$$

We proceed in section II A by a soft-mode analysis of the collinear phase found in the nearest neighbor model. This allows us to identify the stability boundaries of these ground states. Together with a soft-mode analysis of the other Mott-insulating phases with quarter-filling in section II B, this gives the regions in parameter space where intermediate phases (supersolid phases) are to be expected. Using an Ansatz with a general spin configuration on a  $2 \times 2$  unit cell leads us in section II C to an identification of the symmetry of the order parameters in the corresponding non-collinear phases.

## A. Collinear phases

In this section we investigate the collinear phases, i.e. those phases in which the spins are parallel. These are the antiferromagnetic phases, namely the Néel and stripe phase, the paramagnetic phase and the canted-ferromagnetic phase.

### 1. Antiferromagnetic phases: Néel and stripe domain ground states

For vanishing fields, i.e. half-filling, we have a Néel, stripe or a ferromagnetic phase depending on the relative strengths of the interaction parameters  $U_1, U_2$  and  $J$ . In the antiferromagnetic phases (Néel or stripe) the spins are oriented along the  $z$ -axis, which corresponds to an Ising-like anisotropy. Anticipating such a commensurate structure with ordering wave vector  $\tilde{q}$ , which is  $q_0 = \pi(1, 1)$  for the Néel and  $q_1 = \pi(0, 1)$  or  $q_2 = \pi(1, 0)$  for the stripe phase, a Holstein-Primakoff transform yields the spin-wave Hamiltonian

$$\mathcal{H}_{\text{sw}} = E_g + \sum_q \left[ A_q a_q^\dagger a_q + \frac{B_q}{2} (a_q a_{-q} + a_q^\dagger a_{-q}^\dagger) + \frac{h}{2} (a_q^\dagger a_{q+\tilde{q}} + a_{q+\tilde{q}}^\dagger a_q) \right]. \quad (2.3)$$

The coefficients of the Hamiltonian read

$$A_q = S[2(U_1 \tilde{q} + U_2 \tilde{q}) - J_q - J_{q+\tilde{q}}], \quad (2.4a)$$

$$B_q = S(J_{q+\tilde{q}} - J_q). \quad (2.4b)$$

For the Néel phase there are only two ground states, whereas four ground states with the same classical energy

exist for the stripe phase. Diagonalization of the spin-wave Hamiltonian, Eq. 2.3, gives the classical ground state energies

$$E_g = \begin{cases} -4NS^2(U_1 - U_2), & \text{Néel} \\ -4NS^2U_2, & \text{Stripe} \end{cases}, \quad (2.5)$$

and the corresponding two branches of the spin-wave spectra  $\epsilon_q^\pm = \epsilon_q \pm h$  with

$$\epsilon_q = 8S \begin{cases} \sqrt{(U_1 - U_2)^2 - J^2\gamma_q^2} \\ \sqrt{(U_2 - \frac{J}{2}\cos q_x)^2 - \frac{1}{4}J^2\cos^2 q_y} \end{cases}, \quad (2.6)$$

where we have picked the ordering wave vector  $q_1$  for the stripe domain phase. If one takes  $q_2$  instead, then the corresponding excitation spectrum is obtained from Eq. 2.6 by interchanging  $q_x$  with  $q_y$ .

Thus, when comparing the ground state energies, there is a transition from the Néel state to the stripe state at

$$U_2 = U_1/2. \quad (2.7)$$

Since the two ground states have different symmetry the transition is discontinuous (there is no intermediate spin orientation in a mean field approximation and from spin-wave analysis). The domain of stability of each of these classical ground states can be estimated from a soft-mode analysis within linear spin-wave theory. The energy needed to excite a spin-wave at wave vector  $q$  in the collinear phases is given by Eq. 2.6. By increasing the field  $h$  a point can be reached where the lower branch of the excitation energy vanishes at a certain wave vector  $q$ . As a consequence, the spin-wave at this particular wave vector becomes soft, the classical ground state under consideration becomes unstable, and a phase transition to a new phase takes place. Here the minimum in the lower branch of the excitation energies is reached at the Brillouin zone center ( $q = 0$ ) for both ground states. The corresponding upper stability boundaries for the antiferromagnetic (af) zero-field ground states are given by

$$h_{\text{af}}^{\text{max}} = \begin{cases} 8S\sqrt{(U_1 - U_2)^2 - J^2}, & \text{Néel} \\ 8S\sqrt{U_2(U_2 - J)}, & \text{Stripe} \end{cases}. \quad (2.8)$$

For fields  $h$  lower than  $h_{\text{af}}^{\text{max}}$  the Néel and stripe domain phases are stable against quantum fluctuations. Note that in the stripe phase the parameter  $U_1$  does not occur explicitly in the ground state energy and in the spin-wave spectrum.

For  $h < h_{\text{af}}^{\text{max}}$  the dispersion relation shows an energy gap for both phases because there is no continuous degeneracy of the ground state. Thus, these phases have long-range order even at finite temperatures. At  $T = 0$  the order parameter (staggered magnetization) is reduced by quantum fluctuations

$$N = g\mu_B NS \left[ 1 - \frac{1}{2NS} \sum_q \left( \frac{A_q}{\epsilon_q} - 1 \right) \right], \quad (2.9)$$

with  $\epsilon_q$  from Eq. 2.6. From the latter we conclude that this reduction is independent from the field, too. Calculating the magnetization we readily see that there is no contribution from quantum fluctuations; thus, the magnetization vanishes in the whole lobe. This corresponds to a constant mean particle number  $\langle n \rangle \simeq \langle S^z \rangle$ , which is a signature of a Mott insulator. The tip of the lobes of the antiferromagnetic phases can be found from the zeros of the critical fields, Eq. 2.8. The corresponding limits for the hopping integrals are

$$J < \begin{cases} U_1 - U_2, & \text{for checkerboard symmetry,} \\ U_2, & \text{for stripe symmetry.} \end{cases} \quad (2.10)$$

## 2. Paramagnetic phase

In the paramagnetic phase all spins are oriented along the field direction ( $z$ -direction). Applying the Holstein-Primakoff transform we get the following spin-wave Hamiltonian

$$\mathcal{H}_{\text{sw}} = E_g + \sum_q \epsilon_q a_q^\dagger a_q, \quad (2.11)$$

with the classical ground state energy  $E_g$  and the spin-wave spectrum  $\epsilon_q$

$$E_g = 4NS^2(U_1 + U_2) - NSh, \quad (2.12)$$

$$\epsilon_q = h - 2S(U_{10} + U_{20} + J_q). \quad (2.13)$$

Stability of the ground state requires a positive excitation spectrum which gives the lower bound of the paramagnetic phase (soft-mode for  $q = 0$ )

$$h_{\text{min}}^{\text{para}} = h_c = 8S(U_1 + U_2 + J). \quad (2.14)$$

## 3. Canted-ferromagnetic phase

For vanishing field and large values of  $J$  the spins align ferromagnetically in the plane. Due to the rotation symmetry in the  $xy$ -plane there is a Goldstone mode. For an infinitesimal field perpendicular to the plane this ferromagnetic phase becomes unstable and changes to a canted phase where the spins orient ferromagnetically towards the field direction. By minimizing the energy we get a relation between the canting angle and the magnetic field

$$h = h_c \sin \theta. \quad (2.15)$$

Here  $\theta$  denotes the angle between the plane and the spin direction. The resulting ground state energy can be written as

$$E_g = -4NS^2J - NS\frac{h^2}{2h_c}, \quad (2.16)$$

and the dispersion relation for the canted-ferromagnetic state is

$$\epsilon_q^2 = 4S^2(J_0 - J_q) \left[ J_0 - J_q + (J_q + U_{1q} + U_{2q}) \left( 1 - \frac{h^2}{h_c^2} \right) \right]. \quad (2.17)$$

By comparing the classical ground state energy of the paramagnetic and the canted-ferromagnetic phase one finds that the transition to the paramagnetic phase takes place at  $h = h_c$ . This agrees with the lower stability boundary, Eq. 2.14, obtained from a soft-mode analysis of the paramagnetic phase. At the transition the canting angle  $\theta$  continuously goes to  $\pi/2$ . Thus, in a mean-field approximation the corresponding phase transition at  $h = h_c$  is of second order and belongs to the  $D = 3$  classical XY universality class.

The lower field boundary can again be obtained from a soft-mode analysis of the excitation spectrum. One finds that depending on the relative magnitude of the next-nearest and nearest neighbor interaction there is a soft-mode either at the ordering wave-vector of the Néel state  $q = q_0$  or of the stripe domain state  $q = q_1, q_2$ . This gives

$$h_{\min}^{\text{Néel}} = h_c \sqrt{\frac{U_1 - U_2 - J}{U_1 - U_2 + J}}, \quad \text{for } q_0, \quad (2.18a)$$

$$\simeq 8S(U_1 + U_2) - 16S \frac{U_2}{U_1 - U_2} J, \quad (2.18b)$$

and

$$h_{\min}^{\text{stripe}} = h_c \sqrt{\frac{U_2 - J}{U_2}}, \quad \text{for } q_1, q_2. \quad (2.19a)$$

$$\simeq 8S(U_1 + U_2) + 4S \frac{U_2 - U_1}{U_2} J. \quad (2.19b)$$

At these boundaries the canted-ferromagnetic phase becomes unstable to an intermediate phase with a checkerboard or stripe-like spin configuration which will be discussed in section II C. Here we added the expansion for small  $J$ .

### B. The Mott-insulating 3/4 and 1/4 lobe

In the preceding section we have seen that there must be intermediate phases with a more complicated spin configuration. As shown in previous work [9], there exist phases with non-integer filling, namely 3/4 and 1/4, i.e. 3 up and 1 down spin and vice versa for a reversed magnetic field. The spins have no component in the plane. Such a ground state on a square lattice corresponds to a *four-sublattice* system for which the ground state is uniquely defined. By symmetry arguments the down spin (3/4

lobe) can be at each position without changing the energy. The classical ground state of this configuration is given by

$$E_g = -\frac{1}{2}NSh, \quad (2.20)$$

which is independent of the exchange energy  $J$ ,  $U_1$  and  $U_2$ . Performing a spin-wave analysis we can calculate the excitation energy of four branches. From stability conditions, i.e. positiveness of the excitation energies, we can deduce various equations. For  $J = 0$  the Hamiltonian is already diagonal and the four branches of the dispersion relation are given by (s. appendix)

$$\epsilon_q^{(1)} = h - 8SU_2, \quad (2.21a)$$

$$\epsilon_q^{(2)} = h + 8S(U_2 - U_1), \quad (2.21b)$$

$$\epsilon_q^{(3)} = -h + 8S(U_2 + U_1), \quad (2.21c)$$

$$\epsilon_q^{(4)} = h - 8SU_2. \quad (2.21d)$$

These excitations are independent of the wave vector  $q$ . From these equations we get an upper and two lower bounds of the 3/4-lobe, depending on the relative strength of  $U_1$  and  $U_2$ :

$$8S(U_1 + U_2) \geq h \geq \begin{cases} 8S(U_1 - U_2), & U_1 > 2U_2 \\ 8SU_2, & U_1 < 2U_2 \end{cases}. \quad (2.22)$$

The 3/4 phase vanishes for vanishing  $U_2$ . The location of the lower bounds are different, depending on whether the zero-field ground state possesses checkerboard or stripe domain symmetry. For finite  $J$  one has to solve the full dynamical matrix. Vanishing of this spectrum at  $q = 0$  leads to the following condition (see appendix A)

$$h^3 - 8S(2U_1 + U_2)h^2 + (8S)^2(U_1^2 - U_2^2 + 2U_1U_2)h + (8S)^3U_2(U_2^2 - U_1^2 + J^2) = 0, \quad (2.23)$$

which determines three solutions. The fourth solution defines the boundary  $h = 8SU_2$ , which corresponds to  $\epsilon^{(4)}$  and is independent of  $J$ . To see which solutions are relevant we expand them for small  $J$  values:

$$h^{(1)} \simeq 8SU_2 + \frac{8SU_2}{U_1(2U_2 - U_1)} J^2 \quad (2.24a)$$

$$h^{(2)} \simeq 8S(U_2 - U_1) + \frac{4S}{U_1 - 2U_2} J^2 \quad (2.24b)$$

$$h^{(3)} \simeq 8S(U_1 + U_2) - \frac{4S}{U_1} J^2 \quad (2.24c)$$

$$h^{(4)} = 8SU_2. \quad (2.24d)$$

From these expansions we see that  $h^{(3)}$  defines the upper boundary and  $h^{(1)}$  and  $h^{(2)}$  the lower boundaries for the stripe and the Néel ground states respectively.  $h^{(4)}$  is irrelevant. As will be shown in the next section, the lower boundaries  $h^{(1)}$  and  $h^{(2)}$  define a continuous transition to a non-collinear three-sublattice structure (SS2).

In comparison with the phase boundaries for the collinear spin phases (Eq. 2.10) we readily see that the antiferromagnetic phases only meet the 3/4 phase at  $J = 0$ . However, the upper boundary needs some more investigation: the phase boundaries from the canted-ferromagnetic to a non-collinear phase (Eqs. 2.18b and 2.19b) show that the 3/4 phase intrudes (for  $U_2 < U_1$ ) in the canted ferromagnetic phase. The solution of this seemingly paradoxical situation is that there is a discontinuous transition from 3/4 to the canted-ferromagnetic phase, (for low  $J$ ) which is given by the equality of their ground state energies:

$$\begin{aligned} h_{c3} = & 4S(U_1 + U_2 + J) \\ & + 4S\sqrt{(U_1 + U_2 + J)(U_1 + U_2 - 3J)} \\ \simeq & 8(U_1 + U_2) - \frac{8S}{U_1 + U_2}J^2. \end{aligned} \quad (2.25)$$

Thus, for  $U_2 < U_1$  this discontinuous transition is preferred and the upper boundary ( $h^{(3)}$ ) defines a continuous transition to a supersolid phase (SS2) only for  $U_2 > U_1$ .

### C. Non-collinear phases: supersolids

The stability analysis in the preceding sections has shown that there must be several non-collinear phases between the paramagnetic and the Néel/stripe phase in which the spins have both a ferromagnetic and an anti-ferromagnetic orientation. In order to describe these intermediate phases we use an Ansatz with a general spin configuration with four different angles  $\alpha_i$  between the  $z$ -axis and the  $xy$ -plane,  $i = 1, \dots, 4$ , in a  $2 \times 2$  unit cell (see Fig. 2).

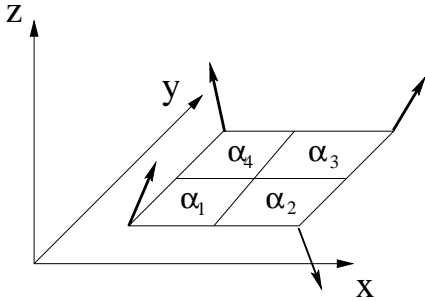


FIG. 2. General spin configuration with four different angles  $\alpha_i$ ,  $i = 1, \dots, 4$ , in a  $2 \times 2$  unit cell.

Due to the planar symmetry only these angles are independent. In such a general four-sublattice model the ground state energy is given by

$$\begin{aligned} E_g = & -\frac{NS^2}{2} \left[ J \sum_{(i,j) \in n.N.} \cos \alpha_i \cos \alpha_j - U_1 \sum_{(i,j) \in n.N.} \sin \alpha_i \sin \alpha_j \right. \\ & \left. - 2U_2 \sum_{(i,j) \in n.n.N.} \sin \alpha_i \sin \alpha_j \right] - \frac{1}{4}hS \sum_{i=1}^4 \sin \alpha_i, \end{aligned} \quad (2.26)$$

where the sums run over the nearest neighbor ( $\sum_{n.N.}$ ) and next-nearest neighbor ( $\sum_{n.n.N.}$ ) sites within the  $2 \times 2$  unit cell.

#### 1. Two-sublattice supersolid phases: SS1 and SS1\* phase

Starting from a general spin configuration with four different angles on a  $2 \times 2$  unit cell there are two different possibilities for a general two-sublattice structure. Corresponding to the Néel and the stripe domain zero-field structure one may have spin configurations with checkerboard ( $\alpha_1 = \alpha_3 = \alpha$ ,  $\alpha_2 = \alpha_4 = \beta$ ) and stripe symmetry ( $\alpha_1 = \alpha_2 = \alpha$ ,  $\alpha_3 = \alpha_4 = \beta$  or  $\alpha_1 = \alpha_4 = \alpha$ ,  $\alpha_2 = \alpha_3 = \beta$ ), which we term SS1 and SS1\*, respectively (see Fig. 3).

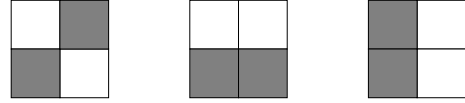


FIG. 3. Sketch of the checkerboard and stripe symmetry. The left figure corresponds to SS1 and the two right ones to SS1\*. The four squares represent the four spin angles  $\alpha_1$ - $\alpha_4$ , where the same color means the same angle.

Using such a two-sublattice Ansatz the corresponding ground state spin configuration is obtained by minimizing the classical energy, Eq. 2.26. This gives the two angles  $\alpha$  and  $\beta$  as a function of the magnetic field  $h$  and the interaction parameters. By comparing the resulting ground state energy with the corresponding ground state energies of the Néel, canted-ferromagnetic and 3/4 phase upper and lower bounds for the stability of the supersolid phase can be obtained. In order to show that these bounds are actually phase boundaries, they must be compared with the results obtained from a soft-mode analysis. Furthermore, it must be determined whether there are additional intermediate phases with a spin structure more general than the two-sublattice Ansatz discussed in this subsection.

After those general remarks, let us now discuss the explicit results from such a mean-field analysis in the various parameter regions.

(i) For  $U_1 > 2U_2$  the checkerboard structure is energetically preferred, i.e. we expect a phase transition from the Néel phase to the intermediate phase SS1. With the introduction of sum and difference angles

$$\gamma = \frac{\alpha + \beta}{2}, \quad (2.27)$$

$$\delta = \frac{\alpha - \beta}{2}, \quad (2.28)$$

minimization of the classical energy leads to a spin configuration described by the angles

$$\sin^2 \gamma = \frac{1}{16SU_2} \sqrt{\frac{U_1 - U_2 - J}{U_1 - U_2 + J}} (h - E_0), \quad (2.29)$$

$$\cos^2 \delta = \frac{1}{16SU_2} \sqrt{\frac{U_1 - U_2 + J}{U_1 - U_2 - J}} (h - E_0). \quad (2.30)$$

The ground state energy reads

$$E_g = -\frac{N}{32U_2} [(h - E_0)^2 + 2(8S)^2 U_2 (U_1 - U_2)], \quad (2.31)$$

where

$$E_0 = 8S \sqrt{(U_1 - U_2 - J)(U_1 - U_2 + J)}. \quad (2.32)$$

Comparing with the ground state energy of the Néel phase, Eq. 2.5, one gets the lower bound of stability of the SS1 phase

$$h_{c1} = E_0 = 8S \sqrt{(U_1 - U_2 - J)(U_1 - U_2 + J)}, \quad (2.33)$$

which is identical to the upper stability boundary obtained from a soft-mode analysis of the Néel phase, Eq. 2.8. Therefore, one may conclude that this is the actual phase boundary between the Néel and SS1 phase, and the corresponding phase transition is continuous (at the mean-field level). The high-field boundary to the canted-ferromagnetic phase is obtained by comparing with the corresponding classical ground state energy of the canted-ferromagnetic phase, Eq. 2.16, or more conveniently by the condition  $\alpha = \beta$ . One finds

$$h_{c2} = h_c \sqrt{\frac{U_1 - U_2 - J}{U_1 - U_2 + J}}, \quad (2.34)$$

which agrees with the lower stability bound obtained from a soft-mode analysis of the canted-ferromagnetic phase, Eq. 2.18b. Hence, this is again an actual phase boundary marking a continuous transition between the canted-ferromagnetic and the supersolid SS1 phase. Of course, this conclusion is valid only if the transition is not pre-empted by a transition of the canted-ferromagnetic phase to another phase which is lower in energy than the SS1 phase. As already seen in the previous section there is a discontinuous transition from 3/4 phase to the canted-ferromagnetic phase for low  $J$  values. The two phase-boundaries meet at the multicritical point  $mc_1$  (s. Figs. 5 and 6) determined by the implicit equation  $h_{c2} = h_{c3}$ . Finally, by comparing the classical ground state energies of the SS1 and the 3/4 phase one obtains the stability boundaries

$$h_{c4}^{\pm} = E_0 + 8SU_2 \pm \sqrt{16SU_2(E_0 + 4S(3U_2 - 2U_1))}. \quad (2.35)$$

Due to different symmetries (two-sublattice for the SS1 and three-sublattice for the 3/4 phase) this transition is discontinuous. This transition can appear only for  $J$  larger than the values at the multicritical point  $mc_1$ . It meets the phase boundaries  $h_{c2}$  and  $h_{c3}$  at  $mc_1$  and  $h_{c1}$

at  $J = 0$  for a certain region of the parameters  $U_1$  and  $U_2$ . Without a stability analysis of the SS1 phase, it is at this point not possible to conclude that the line defined by Eq. 2.35 is an actual phase boundary. As we will see in the following sections the conclusion depends on the actual choice of the parameters  $U_1, U_2$  and  $J$ .

(ii) For  $U_1 < 2U_2$  the low-field phase is the antiferromagnetic stripe phase. The analog intermediate phase (SS1\*) has a ground state energy of

$$E_g = -\frac{N}{16(U_1 + J)} [(h - E_0^*)^2 + (8S)^2 U_2 (U_1 + J)] \quad (2.36)$$

with

$$E_0^* = 8S \sqrt{U_2(U_2 - J)}. \quad (2.37)$$

Here the lower boundary,  $h = E_0^*$ , equals Eq. 2.8 and the upper boundary is

$$h_{c2}^* = h_c \sqrt{\frac{U_2 - J}{U_2}}, \quad (2.38)$$

which agrees with Eq. 2.19b. In the limit of small  $J$  values this transition is given by

$$h_{c2}^* \approx 8S(U_1 + U_2) + 4S \frac{U_2 - U_1}{U_2} J - \frac{S(U_1 + 5U_2)}{U_2^2} J^2. \quad (2.39)$$

Thus, the slope is positive for  $U_2 > U_1$ , in contrast to all the other transition lines at this point (except  $h_{\min}^{\text{para}}$ ). We will see later that this influences the topology of the phase diagram.

The relation between the angles and the field is in analogy to the checkerboard case

$$\sin^2 \gamma = \frac{1}{8S(U_1 + J)} \sqrt{\frac{U_2 - J}{U_2}} (h - E_0^*), \quad (2.40)$$

$$\cos^2 \delta = \frac{1}{8S(U_1 + J)} \sqrt{\frac{U_2}{U_2 - J}} (h - E_0^*). \quad (2.41)$$

Performing a stability analysis of both phases via linear spin-wave theory (see appendix B) shows the occurrence of another phase, a three-sublattice phase SS2. The excitation spectrum for the SS1 phase has a soft-mode at  $q = \pi(1, 0)$  and  $q = \pi(0, 1)$ , whereas the SS1\* has a soft-mode at  $q = \pi(1, 1)$ . The transition line has been determined numerically from the expressions in the appendix. The soft-mode indicates a continuous transition. However, the analysis of the SS2 phase in the next section shows that this is only partially true.

## 2. Three-sublattice supersolid phase: SS2 and SS2\*

From spin-wave considerations in the last section we encountered another phase which has to be more complicated than the general two-sublattice structure. Therefore we are led to consider a three-sublattice structure (SS2 phase) and calculate the phase boundaries to the other phases discussed above. We take the following parameterization of the angles (s. Fig. 4)

$$\alpha_3 = \alpha_1 = \alpha, \quad \alpha_2 = \eta + \zeta, \quad \alpha_4 = \eta - \zeta, \quad (2.42)$$

which has partially a checkerboard symmetry.

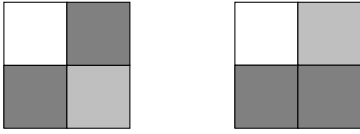


FIG. 4. Sketch of the checkerboard and stripe symmetry. The left figure corresponds to SS2 and the right one to SS2\* which is not stable in a four-sublattice model. The four squares represent the four spin angles  $\alpha_1$ - $\alpha_4$ , where the same color means the same angle.

Inserting in the general four-sublattice expression (Eq. 2.26) for the ground state we can evaluate the mean-field equations for the angles and the resulting ground state energy. Assuming a continuous transition from the SS2 phase in the  $3/4$  phase we recover the result already found for the  $3/4$  phase by spin-wave analysis, Eq. 2.23. This equation, as already discussed, defines only partially a continuous transition. Searching for a continuous transition to the SS1 phase by comparing the corresponding ground state energies we obtain the following equation

$$hU_2E_0 \sin(\gamma - \delta) = 8S[U_1(U_1 - U_2) - J^2]h + 8S(U_2^2 - U_1^2 + J^2), \quad (2.43)$$

which defines the same boundary as found numerically by the spin-wave analysis of the SS1 phase. The angles  $\gamma$  and  $\delta$  are given by the solution for the SS1 phase (Eq. 2.30). Investigation of the ground state by numerical minimization (simulated annealing, see next subsection) of the ground state energy, Eq. 2.26, shows that there are regions where the transition is continuous and regions where the transition is discontinuous. We also find that there is no continuous transition to the SS1\* phase possible due to the different symmetry.

A corresponding SS2\* spin structure with stripe symmetry can be parameterized by (s. Fig. 4)

$$\alpha_2 = \alpha_1 = \alpha, \quad \alpha_3 = \eta + \zeta, \quad \alpha_4 = \eta - \zeta. \quad (2.44)$$

Numerical investigation shows that this phase seems to be absent in the whole parameter range. Within our numerical resolution we could not find any significance for it. From symmetry considerations we expect that there

is no phase of that kind. There are only three different two-sublattice wave-vectors  $q_0, q_1$  and  $q_2$  with which we cannot construct the symmetry of a SS2\* phase.

## 3. Four-sublattice supersolid phase: SS3

In order to study the general four-sublattice structure we have employed two different kinds of numerical methods. Using a simulated annealing code we have determined the ground state spin configurations on the  $2 \times 2$  unit cell; these simulations were crosschecked by a standard library for solving nonlinear equations. We find that the general four-sublattice structure appears only for  $U_1 < 2U_2$ , i.e. for the stripe phase ground state. Thus we find an *intermediate supersolid phase (SS3)*, which interpolates between the SS1\* and SS2 phase such that both transitions become continuous. The resulting phase diagrams are shown in the next section for various values of the interaction parameters  $U_1, U_2$  and  $J$ .

## III. PHASE DIAGRAMS, MULTICRITICAL POINTS AND UNIVERSALITY CLASSES

In this section we summarize our results for the phase diagram of the hard-core Bose-Hubbard model with next-nearest neighbor interaction, as obtained from the linear spin-wave analysis. Furthermore, we identify various multicritical points and comment on the possible universality classes of the phase transitions at the second order phase boundaries.

A number of different phase diagram topologies are possible depending on the relative magnitude of the nearest and next-nearest neighbor interaction. Three different classes may be distinguished. For small values of the next-nearest neighbor interaction,  $U_2 < U_1/2$ , the zero-field ground state is characterized by checkerboard symmetry. In an intermediate range,  $U_1/2 < U_2 < U_1$ , the zero-field ground state switches to stripe symmetry and there is strong competition between nearest and next-nearest neighbor interaction. Finally, the third class of phase diagram topologies is obtained when the next-nearest neighbor interaction is dominant,  $U_2 > U_1$ .

### A. Type I topology: Checkerboard ground state and small next-nearest neighbor interaction ( $U_2 < U_1/2$ )

For relatively small next-nearest neighbor interactions,  $U_2 < U_1/2$ , the classical ground state at zero magnetic field is the Néel state. If the interaction is restricted to nearest neighbors ( $U_2 = 0$ ) there are only three phases: the Néel, the canted-ferromagnetic and the paramagnetic phase (s. Fig. 1). Taking into account longer-range interactions, i.e. for finite  $U_2$ , an additional insulating phase with three quarter filling ( $3/4$  phase) and two supersolid phases, SS1 and SS2, appear [9].



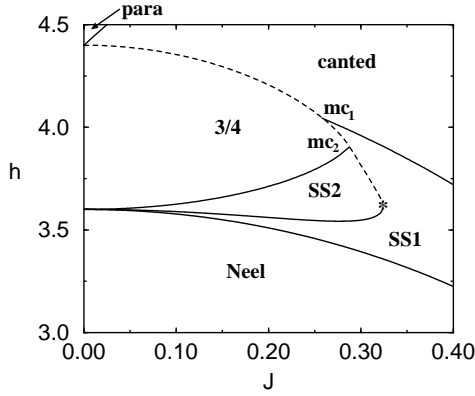


FIG. 5. Part of the phase diagram for the hard-core Bose-Hubbard model for  $U_1 = 1$  and  $U_2 = 0.1$  (cf. [9]). Solid lines indicate continuous phase transitions (to mean-field level), whereas first order phase transitions are given by dashed lines. At finite  $J$  there are four multicritical (mc) points: (i) two critical end points  $mc_1$  and  $mc_2$ , (ii) a tricritical point on the tip of the supersolid SS2 phase (marked by a star (\*)), and (iii) a multicritical point  $mc_3$  on the tip of the Néel phase, which is not shown here.

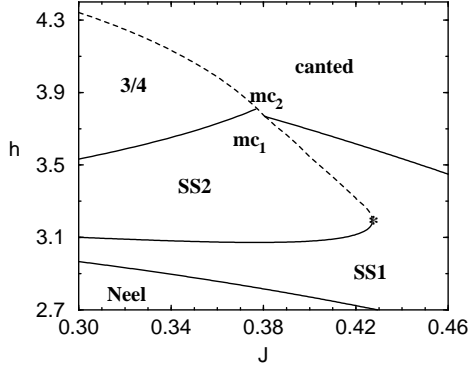


FIG. 6. The same as in Fig. 5 for interaction parameters  $U_1 = 1$  and  $U_2 = 0.2$ .

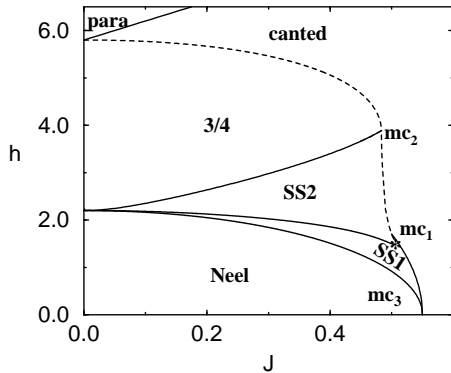


FIG. 7. The same as in Fig. 5 for interaction parameters  $U_1 = 1$  and  $U_2 = 0.45$ .

In Figs. 5–7 we have shown the phase diagrams resulting from ground-state calculations and linear spin-wave analysis for  $U_1 = 1$  and  $U_2 = 0.1$ ,  $U_2 = 0.2$ , and  $U_2 = 0.45$ , respectively. The characteristic features of the mean-field phase diagram are as follows.

(I) *Multicritical points*: At finite values of the hopping matrix element there are four multicritical (mc) points  $mc_1$ ,  $mc_2$ ,  $mc_3$  and the tricritical point on the tip of the SS2 phase (marked by a star in Figs. 5-7). Since for a finite value of the next-nearest neighbor interaction  $U_2$  there is an intermediate supersolid phase intervening the Néel and the canted-ferromagnetic phase, there is a multicritical point  $mc_3$  at the tip of the Néel phase where two second order phase boundaries meet each other with a common tangent. For  $U_2/U_1 \leq 0.183$  the second order line separating the canted-ferromagnetic (i.e. superfluid) from the supersolid SS1 phase intersects and is truncated by a first order phase boundary to the commensurate 3/4 solid phase. The corresponding multicritical point  $mc_1$  is a *quantum critical end point*. The “spectator phase” is the uncritical Mott insulating 3/4 phase. The second *quantum critical end point*  $mc_2$  differs from  $mc_1$  in one important aspect. This time the “spectator phase” is the supersolid SS1 phase characterized by the simultaneous presence of crystalline order and superfluidity. Hence the “spectator phase” is critical since it shares the superfluid order and the corresponding Goldstone mode for the phase of the superfluid order parameter with one of the phases (the SS2 phase) associated with the critical line. Fisher et al. [16,17] have shown that the singular behavior at the critical end point also engenders new singularities in the first order phase boundary itself. Therefore one may speculate that the presence of the critical end point may also affect the “spectating” supersolid phase and induce “non Bose-liquid” behavior.

Upon increasing the relative magnitude of the next-nearest neighbor interaction the two critical end points  $mc_1$  and  $mc_2$  approach each other and for  $U_2/U_1 \approx 0.183$  they merge into a *higher order multicritical point*. The critical values at this point are  $J_c = 0.365$  and  $h_{\text{crit}} = 3.827$ . From a higher dimensional perspective, where the ratio  $U_2/U_1$  is added as an additional axis in the phase diagram, this point corresponds to the crossing point of two multicritical lines. In the projection of this higher dimensional phase diagram,  $mc_1$  and  $mc_2$  switch their relative position for  $U_2/U_1 > 0.183$ : now at  $mc_2$  the 3/4, the canted-ferromagnetic and the SS2, and at  $mc_1$  canted-ferromagnetic, SS1 and SS2 meet.

There is also a tricritical point on the tip of the SS2 phase where the first order line separating the two supersolid phases terminates and becomes second order. The presence of the tricritical point is to be expected, since critical end points in classical critical phenomena are intimately associated with the vicinity of tricritical points [17]. With increasing the next-nearest neighbor interaction the critical end point  $mc_1$  and the tricritical point approach each other. At  $U_2 = U_1/2$  they merge into a higher order multicritical point.

(II) *Supersolid phases*: There are two different supersolid phases, SS1 and SS2, and each of them has a Mott-insulating partner phase with the same symmetry of the charge ordering, the Néel and the 3/4 phase, respectively. The phase transition between the two supersolid phases is first-order at high fields and becomes second-order at low fields. The tricritical point, where those two transition lines meet is located at the tip of the SS2 phase. With increasing  $U_2$  the SS2 phase fills more and more of the parameter region occupied by the SS1 phase (see Fig. 5-7). At  $U_1 = 2U_2$  the phase diagram changes drastically because the stripe phase replaces the Néel phase.

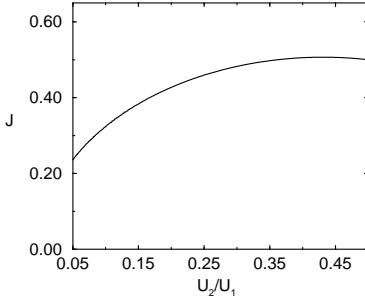


FIG. 8. Location of the tip of the supersolid SS2 phase as a function of the ratio  $U_2/U_1$ . The maximum of the tip is reached before the transition to the stripe ground state, namely for  $U_2/U_1 \simeq 0.43$  with a maximum value of  $J \simeq 0.507$ .

In Fig. 8 a plot is shown for the tip ( $J$ -value, marked by a star in the phase diagrams) of the SS2 lobe as a function of  $U_2/U_1$ . From the soft-mode analysis (see appendix B) of the SS1 phase we can derive a cubic equation which defines the tip by the collapse of two solutions. Surprisingly, the maximum of the tip is reached before the transition to the stripe ground state, namely for  $U_2/U_1 \simeq 0.43$  with a maximum value of  $J \simeq 0.507$ . As it turns out the SS1\* phase intrudes in the area of the SS1 phase for  $U_2$  slightly smaller than 0.5 (s. Fig 18).

(III) *Universality classes*: Whereas the mean-field analysis in section II is certainly sufficient in describing the overall topology of the phase diagram and the ordered phases away from the transition, it breaks down near the phase transition where the correlation length diverges. The critical behavior at the phase transition from the SS1 phase (checkerboard supersolid = XSS) to the canted-ferromagnetic phase (i.e. superfluid phase in the corresponding Bose system) has recently been studied by renormalization group theory [18]. It is found that the phase transition from the checkerboard supersolid to the superfluid phase can be described by an effective action, where an Ising field is coupled to the superfluid phase fluctuations (*XSS-SF universality class*). It exhibits nontrivial critical behavior and appears within an  $\varepsilon$ -expansion to be driven first order by fluctuations. However, within a calculation directly in  $d = 2$  dimensions one finds a fixed-point with “non Bose-liquid” behavior. At the transition between the two supersolid phases

(at low fields) there are soft-modes at  $q_1 = \pi(1,0)$  and  $q_2 = \pi(0,1)$  (see appendix B). Hence the boson density in the SS2 phase may be characterized by

$$n(x) = n_0 \text{Re} \left( 1 + \phi e^{iq_0 x} + \psi_1 e^{iq_1 x} + \psi_2 e^{iq_2 x} \right), \quad (3.1)$$

where  $n_0$  is a background boson density and the fields  $\phi$  and  $\psi$  represent the checkerboard and stripe domain order parameters, respectively. From the mean-field analysis in the preceding section we know that in the SS2 phase, the system orders along the [11]-direction in the  $(\psi_1, \psi_2)$ -plane. This implies a particular form of the cubic anisotropy in the effective action in the SS2 phase ( $v' > 0$ , see below). The XY field  $\psi$  is linearly coupled to the Ising field  $\phi$  describing the checkerboard order of the SS1 phase. The corresponding action allowed by symmetry reads [18]

$$S_0 = \int d\mathbf{x} d\tau \left\{ \frac{1}{2} \left( \frac{1}{c} \partial_\tau \phi \right)^2 + \frac{1}{2} (\nabla \phi)^2 + \frac{t}{2} \phi^2 + \frac{u}{4!} \phi^4 \right. \\ \left. + \frac{1}{2} \left| \frac{1}{c'} \partial_\tau \psi \right|^2 + \frac{1}{2} |\nabla \psi|^2 + \frac{t'}{2} |\psi|^2 + \frac{u'}{4!} |\psi|^4 \right. \\ \left. + \frac{v'}{4!} \sum_i \psi_i^4 + w \phi \prod_i \psi_i + \tilde{w} \phi^2 \sum_i \psi_i^2 \right\}, \quad (3.2)$$

with the control parameters  $t$  and  $t'$  measuring the distances from the critical lines. Within the linear spin-wave theory in section II these critical lines coincide with those curves in parameter space, where the spin-wave spectrum has a soft-mode at the ordering wave vector of the corresponding field. The parameters of the effective action are related to the microscopic parameters of the original Bose-Hubbard model, which may be worked out using a mean-field decoupling procedures (see e.g. the appendix of Ref. [18]). Non-local interactions arise due to interactions with long wavelength fluctuations of the superfluid phase,  $\theta$ ,

$$S_1 = \frac{\tilde{\rho}_s}{2m^2} \int d\mathbf{x} d\tau \left\{ \left( \frac{1}{v} \partial_\tau \theta \right)^2 + (\nabla \theta)^2 \right\}, \quad (3.3)$$

where we have used the same notation as in Ref. [18]. This part of the effective action originates from the  $x$  and  $y$  spin components in the spin-1/2 XXZ model, Eq. 1.2. Sufficiently far from the phase boundary where the superfluid order parameter vanishes, the most relevant coupling to the spatial order parameters allowed by the time-reversal and  $U(1)$  symmetries is [18]

$$S_2 = \int d\mathbf{x} d\tau \left\{ i\sigma \partial_\tau \theta |\phi|^2 + i\sigma' \partial_\tau \theta |\psi|^2 \right\}. \quad (3.4)$$

For the phase transition from the SS1 to the SS2 phase, the spin-wave spectrum softens at the stripe domain ordering wave vectors  $q_1$  and  $q_2$ , i.e.  $t'$  becomes zero. Since this happens in the presence of an already ordered Ising field  $\phi$  there are now two different cubic anisotropies,

the quartic term and the quadratic term,  $g\psi_1\psi_2$ , where  $g = w\langle\phi\rangle$ . Whereas the quartic cubic anisotropy is an irrelevant symmetry breaking field for the XY transition [19], the quadratic symmetry breaking field  $g$  leads to an uniaxial anisotropy in the [11]-direction and hence to a reduction in the number of soft spin components from  $n = 2$  to  $n = 1$ . This in turn implies that the coupling to the phase fluctuations becomes relevant to the asymptotic critical behavior at the SS1 to SS2 phase transition, and the asymptotic critical behavior is in the XSS-SF universality class. When the checkerboard order parameter  $\langle\phi\rangle$  is decreased, the quadratic symmetry breaking field becomes small, and there can be quite interesting crossover phenomena. One should note that here both the cubic and the quartic cubic anisotropy favor spin orientation in the [11]-direction, since  $v' > 0$ . Later we will encounter a case where the cubic anisotropy becomes negative and as a consequence of the competition between these two anisotropies new intermediate supersolid phases appear.

Interesting new quantum critical behavior is also found in the vicinity of the tricritical point at the tip of the supersolid SS2 phase. Since the tricritical point of the classical  $D = 3$   $n$ -vector model is described by classical exponents with logarithmic corrections, the specific heat exponent  $\alpha$  becomes positive,  $\alpha = 2 - D\nu = 0.5$ . As a consequence the coupling to superfluid phase mode becomes even more relevant on approaching the tricritical point. The effective action at the tricritical point reduces to

$$S_0 = \int dx d\tau \left\{ \frac{1}{2} \left| \frac{1}{c'} \partial_\tau \psi \right|^2 + \frac{1}{2} |\nabla \psi|^2 + \frac{t'}{2} |\psi|^2 + \frac{v'_1}{6!} |\psi|^6 + \frac{v'_2}{6!} |\psi|^2 \sum_i \psi_i^4 + \frac{v'_3}{6!} \sum_i \psi_i^6 + g \psi_1 \psi_2 \right\}. \quad (3.5)$$

Due to the positive value of  $\alpha$ , a renormalization group analysis of this *quantum tricritical model* will yield a new universality class different from the  $D = 3$  tricritical Ising model. We leave the corresponding analysis of the asymptotic critical and crossover behavior for a future investigation [20].

Finally, the topology of the phase diagram allows for phase transitions between the supersolid and commensurate solid phases. At both transition the order parameter characterizing superfluid order becomes zero. In passing from the SS1 to the Néel phase the order parameter describing checkerboard ordering changes smoothly, while a two-component field  $\Psi$  describing superfluidity becomes critical. Since generically there is no particle-hole symmetry (charge conjugation) symmetry along this phase boundary [21], the effective action can contain a term  $\Psi^* \partial_\tau \Psi$  which is more relevant than  $|\partial_\tau \Psi|^2$ . Hence, the transition in  $2 + 1$  dimensions becomes mean-field like with logarithmic corrections. Similar conclusions hold for the transition from the SS2 to the 3/4 phase.

## B. Type II topology: Intermediate next-nearest neighbor interaction ( $U_1/2 < U_2 < U_1$ )

In this parameter region the zero-field ground state is an antiferromagnet with a striped structure. As a consequence of the strong competition between nearest and next-nearest neighbor interaction the phase diagram exhibits quite a rich structure with first and second order phase boundaries and various multicritical points. The characteristic features are as follows:

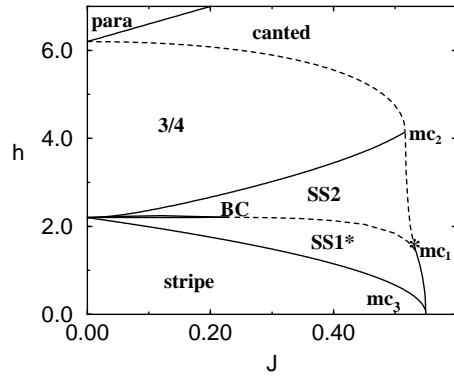


FIG. 9. Phase diagram for the hard-core Bose-Hubbard model with interaction parameters  $U_1 = 1$  and  $U_2 = 0.55$ . The first-order and second-order lines in the phase diagram are depicted by dashed and solid lines, respectively. There are five multicritical points: (i) one critical end point,  $mc_2$ , (ii) two bicritical points, BC and  $mc_1$ , (iii) one tricritical point along the phase boundary between the supersolid SS2 phase and the canted-ferromagnetic phase in the intermediate vicinity of  $mc_1$  (marked by a star (\*)), and (iv) the multicritical point on the tip of the checkerboard solid phase. The small sliver is the SS3 phase.

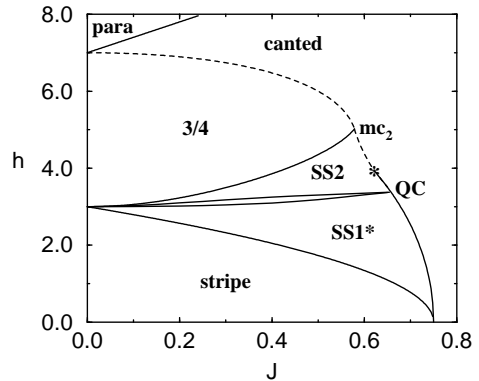


FIG. 10. Phase diagram for the hard-core Bose-Hubbard model with interaction parameters  $U_1 = 1$  and  $U_2 = 0.75$ . The bicritical point on the tip of the SS3 phase has merged with the bicritical  $mc_1$  to form a tetracritical point (QC). Otherwise the phase diagram has the same topology as Fig. 9.

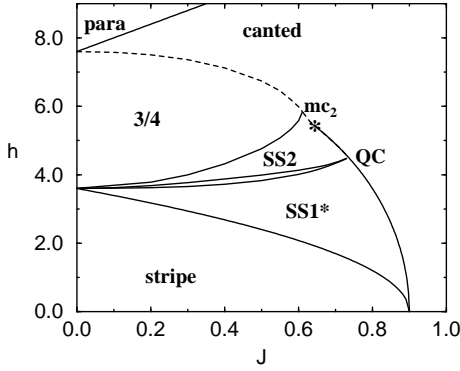


FIG. 11. Phase diagram for the hard-core Bose-Hubbard model with interaction parameters  $U_1 = 1$  and  $U_2 = 0.9$ . The phase diagram has the same topology as Fig. 10. The tricritical point on the phase boundary between the SS2 and the canted-ferromagnetic phase has shifted towards the multicritical point  $mc_2$ .

(I) *Supersolid phases*: There are *three* supersolid phases. In addition to the SS1 and SS2 phase we find an intermediate supersolid phase SS3 characterized by a four-sublattice structure with all four angles on the  $2 \times 2$  unit cell being different. Increasing the next-nearest neighbor interaction  $U_2$  from the lower bound  $U_2/U_1 = 0.5$  a sliver of the SS3 phase appears at small values of the hopping matrix element  $J$  (see Fig. 9). Both of the transitions of the other two supersolid phases to this intermediate supersolid phase are continuous. This can also be inferred from Fig. 12, where the variation of the four angles of the spin configuration are shown as a function of the magnetic field  $h$  for fixed hopping matrix element  $J = 0.40$ .

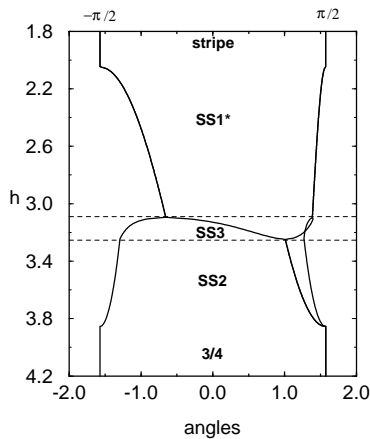


FIG. 12. Variation of the angles on the  $2 \times 2$  unit cell characterizing the spin configuration at fixed interaction parameters  $J = 0.40$ ,  $U_1 = 1$  and  $U_2 = 0.75$  as a function of the magnetic field  $h$ . All transitions are seen to be continuous on the mean-field level. The boundaries of the SS3 supersolid phase are marked by dashed lines.

For larger values of  $J$  the transition is still directly from the SS2 to the SS1\* phase with a jump in the angles of the spin configuration, i.e. the transition is first-order. As the ratio of  $U_2/U_1$  becomes larger the SS3 phase occupies a larger portion in parameter space and finally (at  $U_2/U_1 \approx 0.75$ ) meets with its tip the phase boundary to the canted-ferromagnetic phase. See the topology of the phase diagram in Fig. 10, where  $U_2/U_1 = 0.75$ . For larger values of  $U_2$  the SS3 phase keeps its topology, i.e. there is an intermediate SS3 phase completely separating the SS2 from the SS1\* phase by a series of continuous phase transitions.

(II) *Multicritical points*: Due to the competition between nearest neighbor and next-nearest neighbor interaction there are also several interesting multicritical points. Here we discuss those which appear at finite values of  $J$ . Right at  $U_2 = U_1/2$  the critical end point  $mc_1$  and the tricritical point at the tip of the SS2 phase (compare Fig. 7) have merged into a *tricritical end point*. A slight increase of  $U_2$  above the critical value  $U_1/2$  implies that part of the phase boundary between the SS2 and the canted-ferromagnetic phase becomes a second order line. Then,  $mc_1$  becomes a bicritical point and a new tricritical point close to  $mc_1$  appears (compare Fig. 9). The bicritical point separates two second-order lines from the superfluid to two supersolid phases with distinct ordering wave vectors. The SS1\* phase is characterized by one of the stripe-domain ordering wave vectors  $q_1 = \pi(0, 1)$  or  $q_2 = \pi(1, 0)$ ; the charge ordering in the SS2 phase is more complicated and in addition to  $q_1$  and  $q_2$  requires a third (checkerboard) wave vector  $q_0 = \pi(1, 1)$ . In addition there is a bicritical point (BC) on the tip of the SS3 phase. Upon increasing the next-nearest neighbor interaction the tip of the SS3 phase and hence the bicritical point moves towards the bicritical point  $mc_1$  until both join at the critical value  $U_2^* \approx 0.75$  to a tetracritical point (QC) [22]. At the same time the phase boundary connecting  $mc_1$  and  $mc_2$  becomes more and more of second order. As a consequence the tricritical point shifts toward the critical end point  $mc_2$  (compare Fig. 11). Finally, at  $U_2 = U_1$  the phase boundary between the SS2 and canted-ferromagnetic phase is completely of second order and the tricritical point merges with the critical end point to become a tricritical end point at

$$J_c = g - 1, \quad h_c = 4g, \quad (3.6)$$

where  $g = (1 + \sqrt{5})/2$  denotes the golden mean. The tip of the 3/4 phase is located at  $J_{\text{tip}} = (2/\sqrt{27})^{1/2} > J_c$ . This tip appears for  $U_2 > 0.96$ . At  $U_2 = U_1$  the phase line for smaller  $J$  values is still a discontinuous transition between the canted-ferromagnetic and the 3/4 phase but becomes a complex transition for slightly larger values (subsection C).

(III) *Universality classes*: In each of the three supersolid phases the boson density may again be characterized by

$$n(x) = n_0 \text{Re} (1 + \phi e^{iq_0 x} + \psi_1 e^{iq_1 x} + \psi_2 e^{iq_2 x}). \quad (3.7)$$

For  $U_2/U_1 \leq 0.75$  and large enough  $J$  there is a first order line separating the SS1\* from the SS2 phase. In both phases the stripe domain order parameter  $\psi$  is finite, but differs in its alignment in the  $(\psi_1, \psi_2)$ -plane. Whereas the vector  $\psi$  points along one of the cube edges in the SS1\* phase, it is oriented along one of the cube diagonals in the SS2 phase. From the mean-field analysis in section II we also know that the checkerboard order parameter  $\phi$  is zero in the SS1\* phase but finite in the SS2 phase. Below a certain critical value of  $J$  which depends on the ratio  $U_2/U_1$  there is an intervening supersolid phase (SS3) characterized by an order parameter  $\psi$  which rotates from the cube edges to the cube diagonals as one passes from the SS1\* to the SS2 phase.

The topology of this part of the phase diagram can be understood in terms of a mean-field analysis of the effective action, Eq. 3.2. The phase boundary between the SS1\* phase and the SS3 phase corresponds to  $t = 0$  and the phase boundary between the superfluid phase and both of the supersolid phases corresponds to  $t' = 0$ . The first order transition between the SS1\* and the SS2 phase is a consequence of the competition between the quartic ( $v' < 0$ ) and quadratic ( $w$ ) cubic symmetry breaking fields in the effective action. A mean-field analysis of the latter shows that sufficiently far from the phase boundary  $t = 0$  the first order line is given by the relation  $v'_c = -6w^2/t$ . For  $v' < v_c$  the effective action is minimized by a configuration, where  $\phi = 0$  and  $\psi$  points along one of the cube edges. This is the SS1\* phase. For  $v' < v_c$  both the checkerboard and stripe domain order parameters become finite and  $\psi$  points along one of the cube diagonals, as is the case for the SS2 phase. In particular one finds that at the phase transition from the superfluid to the SS2 phase ordering of the  $\psi$ -field induces ordering in the Ising field  $\phi$ . In mean-field (mf) approximation one gets  $\phi_{mf} = (-w)\langle\psi\rangle^2/t$ , due to the trilinear coupling to the  $\psi$ -field.

The competition between the quartic and quadratic cubic symmetry breaking fields also leads to the existence of an intermediate supersolid phase (SS3). In the SS1\* phase the quartic field  $v' < 0$  dominates and we have alignment along one of the cube edges in the  $(\psi_1, \psi_2)$ -plane. Right at the phase boundary between the SS1\* and the SS3 phase the spin-wave spectrum becomes soft at the checkerboard ordering wave vector  $q_0$  (i.e.  $t = 0$ ). Hence within the SS3 phase we have a finite mean value for the Ising field,  $\langle\phi\rangle \neq 0$ , which implies that in addition to the quartic cubic anisotropy ( $v' < 0$ ) we have a quadratic term,  $g\psi_1\psi_2$  with  $g = w\langle\phi\rangle$ . The latter favors spin alignment along the cube diagonals in the  $(\psi_1, \psi_2)$ -plane, which now starts competing with the quartic symmetry breaking field  $v' < 0$ . By increasing the magnetic field and moving away from the SS1\*-SS3 phase boundary the expectation value of the Ising field  $\phi$  and hence the magnitude of the quadratic symmetry field  $g$  starts to grow leading to a rotation of the spin alignment from the cube edges to the cube diagonals (compare also Fig. 12). When the rotation is completed there is a phase tran-

sition into the SS2 phase. With increasing  $U_2/U_1$  the bicritical point on the tip of the SS3 phase meets with the phase boundary to the canted-ferromagnetic phase and it becomes a tetracritical point [22].

The above symmetry considerations allow us now to discuss the universality classes of the phase transitions between the various supersolid phases and the superfluid phase. Let us first discuss the phase transitions between the superfluid and the supersolid phases. The transition from the superfluid to the SS1\* phase (collinear supersolid = CSS) is in the universality class of the  $D = 3$  classical XY model (*CSS-SF universality class*) [18]. At the second order phase boundary between the superfluid and the SS2 phase (mixed supersolid = MSS) the checkerboard and the stripe domain ordering wave vectors become soft simultaneously. As discussed above, this is not a consequence of both  $t$  and  $t'$  becoming zero at this phase boundary but due to the trilinear coupling between the checkerboard and stripe domain order parameters. Ordering of the stripe domain field  $\psi$  automatically induce ordering of the checkerboard field  $\phi$  (see the above mean-field result). The critical exponent  $\beta_\phi$  for the Ising field is  $\beta_\phi = 1$  already at the mean-field level. Whereas the critical behavior of the XF field seems to be unchanged at the transition, the trilinear coupling induces cusp-like singularities in the “slaved” checkerboard field  $\phi$ . The critical behavior of such a model constitutes a new universality class (*MSS-SF universality class*) and leave a more detailed analysis for a future investigation [20].

Next we consider the universality classes of the phase transitions between the various supersolid phases. By increasing the field  $h$  in the SS1\* phase one may either encounter a first order phase boundary to the SS2 phase or a second order boundary to the SS3 phase. In the latter case the spin-wave spectrum becomes soft at the checkerboard ordering wave vector. Thus the effective action is given by an Ising-field which couples linearly to an XY field which is already ordered along one of the cube edges. After integrating out the  $\psi$  field one is left with an Ising model with renormalized coefficients. Hence this transition belongs to the XSS-SF universality class [18]. In the intermediate supersolid SS3 phase the direction of the XY field  $\psi$  rotates from the cube edge to the cube diagonal. The order parameter for the transition to the SS2 phase is the one-component field  $\sigma = \psi_1 - \psi_2$ . We thus conclude that this transition is again the XSS-SF universality class.

At the multicritical point on the tip of the SS3 phase both of the Ising fields  $\phi$  and  $\sigma = \psi_1 - \psi_2$  become critical. The corresponding *bicritical* effective action for the charge ordering fields is given by

$$S_0^{bc} = \int d\mathbf{x}d\tau \left\{ \frac{1}{2} \left( \frac{1}{c} \partial_\tau \phi \right)^2 + \frac{1}{2} (\nabla \phi)^2 + \frac{t}{2} \phi^2 + \frac{u}{4!} \phi^4 \right. \\ \left. + \left( \frac{1}{c'} \partial_\tau \sigma \right)^2 + \frac{1}{2} (\nabla \sigma)^2 + \frac{t}{2} \sigma^2 + \frac{u'}{4!} \sigma^4 \right\}$$

$$+w\phi\sigma^2\Big\}.$$
(3.8)

Note that this is a rather peculiar effective action for a bicritical point, since it consists of two Ising fields  $\phi$  and  $\sigma$  coupled by a three-point vertex. Since the upper critical dimension of the coupling vertex  $w\phi\sigma^2$  is  $D_c = 6$  as compared to  $D_c = 4$  for the  $\phi^4$  and  $\sigma^4$  vertices the former will dominate the critical behavior. In combination with the coupling to the superfluid phase this should result in quite interesting critical behavior. The effective action bears some resemblance with field theories for anisotropic Potts models [23]. It would, however, go beyond the scope of the present paper to analyze the critical behavior of such a model. But, it certainly constitutes a quite interesting new *quantum bicritical universality class*, which could be analyzed using standard renormalization group theory.

With increasing the next-nearest neighbor interaction  $U_2$  the bicritical point moves towards the phase boundary to the superfluid phase. When it meets at about  $U_2/U_1 = 0.75$  one gets a tetracritical point, where four second order lines meet.

Finally, the phase transition from the supersolid SS1\* phase to the stripe domain solid and from the SS2 phase to the 3/4 phase are both most likely mean-field like with logarithmic corrections in  $D = 2 + 1$  dimensions.

### C. Type III topology: Large next-nearest neighbor interaction ( $U_2 > U_1$ )

For this parameter range the zero-field classical ground state is an antiferromagnet with stripe symmetry. Due to the positive slope of the critical field in the SS1\* phase (Eq. 2.39) the SS2 phase transition splits the discontinuous transition from the canted-ferromagnetic to 3/4 phase into two continuous transitions. For  $U_2 > 1.149$  this transition is established for the whole high field region.

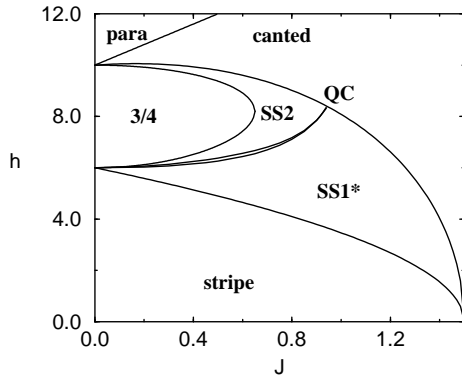


FIG. 13. Phase diagram for the hard-core Bose-Hubbard model with interaction parameters  $U_1 = 1$  and  $U_2 = 1.5$ . The phase in between the SS2 and the SS1\* is the SS3.

(I) *Supersolid phases and topology of the phase diagram:* For values of the next-nearest neighbor interaction in the range of  $1.149 < U_2/U_1 \lesssim 3$  (see Fig. 13) there are three different supersolid phases, SS1\*, SS2, SS3. The SS3 phase is located in the thin sliver between the SS2 and SS1\* phase. Due to the presence of the intermediate SS3 supersolid phases all phase transitions are continuous. The transition from the SS2 phase directly to the canted-ferromagnetic phase without passing the SS1\* phase has also quite interesting properties. Surprisingly, the transition line is given by

$$h = h_c \sqrt{\frac{U_2 - J}{U_2}}, \quad (3.9)$$

the same dependence as for the transition of canted-ferromagnet to SS1\*.

The topology for  $1 < U_2/U_1 < 1.149$  is similar to the just described one but with a slight change for the high field transition between the canted-ferromagnetic and the 3/4 phase. When comparing the phase transition between the canted-ferromagnetic and the 3/4 (Eq. 2.26), the canted-ferromagnetic and the SS2 (Eq. 3.9) and the 3/4 and the SS2 (Eq. 2.23) we encounter various region (as a function of  $J$ ) where the SS2 phase occurs. In the region for  $U_2/U_1 < 1.124$  we have for increasing  $J$  the following picture (Fig. 14): There is a SS2 phase between the canted and the 3/4 (continuous on both transitions), then a SS2 phase with a discontinuous transition to the 3/4 phase, a direct transition from canted-ferromagnetic to 3/4, a SS2 with discontinuous transition to the 3/4 again and for high values of  $J$  the SS2 phase with continuous transitions to either phases.

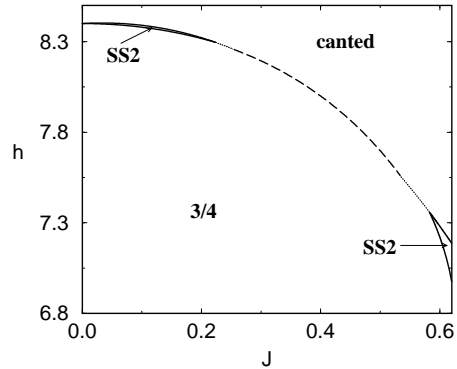


FIG. 14. Phase diagram for the hard-core Bose-Hubbard model with interaction parameters  $U_1 = 1$  and  $U_2 = 1.1$ . The dashed transition line defines a discontinuous transition from canted-ferromagnetic to 3/4, the solid lines for small  $J$  denotes two second order transition, namely from canted-ferromagnetic to SS2 and then to 3/4. The dotted lines denote a discontinuous transition from canted-ferromagnetic to SS2 and a continuous transition from SS2 to 3/4. The actual phase cannot be resolved on this scale.

The direct transition from canted-ferromagnetic to 3/4 vanishes for  $U_2/U_1 \geq 1.124$  at  $J = 0.415$ . For  $U_2/U_1 > 1.149$  only the SS2 phase with the continuous transitions keeps established. This happens for a critical value of  $J = 0.45$ . Equality of Eq. 2.38 and Eq. 2.26 define those multicritical points where the canted to 3/4 and the canted to SS2 phase lines meet. They are given by the two positive solutions of (besides  $J = 0$ )

$$J^3 + (2U_1 - U_2)J^2 + U_1(U_1 - 2U_2)J + U_2(U_2^2 - U_1^2) = 0.$$

For large values of next-nearest neighbor interaction,  $U_2/U_1 > 3.1$ , the phase diagram has a topology as depicted in Fig. 15 for the particular value of  $U_1 = 1$  and  $U_2 = 5$ . The SS2 phase is now completely surrounded by the SS1\* phase and there is no direct transition from the SS2 phase to the canted-ferromagnetic phase anymore. The tip of the SS2 lobe can be calculated analytically from the soft-mode of the SS1\* phase (s. appendix B). It turns out that the value for  $J_{\text{tip}}$  has a remarkably simple form, namely

$$J_{\text{tip}} = U_1. \quad (3.10)$$

In the extreme limit of vanishing nearest neighbor interaction,  $U_1 = 0$ , only the SS1\* phase as a supersolid phase survives. The other supersolid phases and the 3/4 Mott insulator phase disappear (s. Fig. 16).

(II) *Multicritical points and universality classes:* The number of multicritical points in this parameter range is reduced. For  $U_2/U_1 \lesssim 3.1$  there is a tetracritical point at the intersection point of the three supersolid phases (QC). This multicritical point disappears for  $U_2/U_1 \gtrsim 3.1$  and there is a tricritical point at the tip of the SS2 phase instead. Furthermore there is a multicritical point at the tip of the Néel phase. The properties of all of these multicritical points have already been discussed in the preceding subsections. There are also no new universality classes in the phase diagram which have not already been discussed.

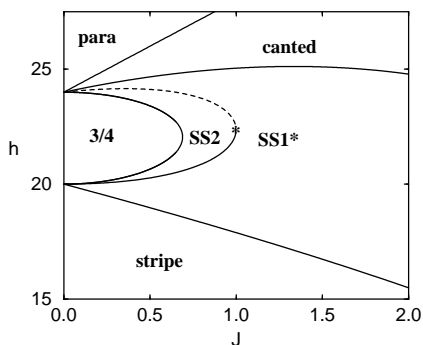


FIG. 15. Phase diagram for the hard-core Bose-Hubbard model for  $U_1 = 1$  and  $U_2 = 5$ . The SS3 phase, which is located between the SS2 and the SS1\* (lower fields) cannot be resolved at this scale.

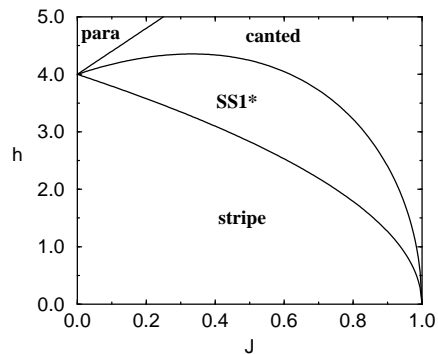


FIG. 16. Phase diagram for the hard-core Bose-Hubbard model for pure next-nearest interaction,  $U_2 = 1$  and  $U_1 = 0$ . Note that there is only one supersolid phase (SS1\*).

#### IV. SUMMARY AND CONCLUSIONS

The analysis of the hard-core Bose-Hubbard model with nearest and next-nearest neighbor interaction on a square lattice presented in this paper has demonstrated that the phase diagram can exhibit a rich variety of new quantum critical and multicritical phenomena. The topology of the phase diagram is determined by the interplay between the nearest and next-nearest charge interaction of the bosons and the cubic anisotropy. The principal effect of these terms is to stabilize several supersolid phases, which are characterized by the simultaneous presence of superfluidity and charge ordering, where the latter was described in terms of an Ising and a XY field.

*Topology of the phase diagram:* We investigated the whole parameter range for nearest ( $U_1$ ) and next-nearest neighbor ( $U_2$ ) interaction. By using ground state energy calculations and stability analysis (spin-wave theory) we have derived the phase diagrams in mean-field approximation plus small fluctuations. It turns out that there are three main types of phase diagram topologies. In parameter regions ( $U_1 > 2U_2$ ), where the Néel ground state is established at zero field (half-filling), we encounter two supersolid phases, as already stated by Bruder et al. [9], a superfluid phase, and three different types of Mott insulating phases. Whereas the spatial order of the supersolid SS1 phase can be described solely in terms of a checkerboard pattern, the second supersolid phase (SS2) is a superposition of checkerboard and stripe domain density waves. In the region where a stripe ground state at half-filling is favored ( $U_2 > U_1/2$ ) three supersolid phases are found, SS2, SS3 and SS1\*. The SS1\* phase is the “supersolid partner” of the commensurate solid with a stripe domain structure and the spatial structure of its boson density can solely be described in terms of the stripe domain ordering wave vectors  $q_1 = \pi(1,0)$  and  $q_2 = \pi(0,1)$ . The phase transition from the SS1\* to the SS2 phase is either continuous or first order, depending on the particular choice of parameters. In terms of an effective action this can be restated as follows. The phase

transition from the SS1\* to the SS2 phase is split up into two phase transitions with an intervening supersolid SS3 phase, if the Ising field describing the checkerboard structure orders before the first order transition occurs; otherwise the phase transition is first order. The transition from the Mott insulator phase (3/4) is of second order into the SS2. For  $U_2 < U_1$  the 3/4 phase joints partly (for higher fields) the canted-ferromagnetic phase; the transition is discontinuous. The occurrence of the supersolid phases is strictly coupled to a finite value of  $U_2$ . Even in the limit of vanishing nearest neighbor interaction,  $U_1 = 0$ , there is the SS1\* supersolid phase present. It is also quite remarkable to note that in the parameter range  $1.149 < U_2/U_1 \lesssim 3$  the transition line from the canted ferromagnetic to the SS2 phase is the same as for the transition from the canted ferromagnetic phase to the SS1\* phase over the whole range of hopping matrix elements  $J$ .

Figs. 17-18 show the complex topology of the phase diagram for fixed hopping matrix elements but varying strength of the next-nearest neighbor interaction.

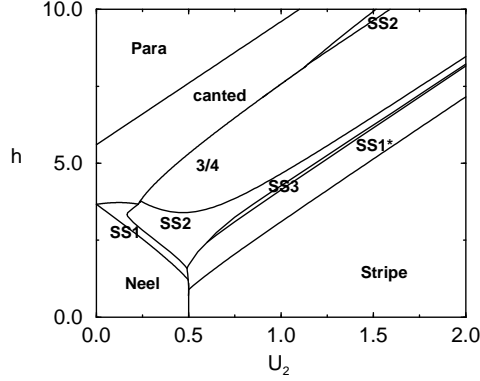


FIG. 17. Phase diagram for the hard-core Bose-Hubbard model with  $U_1 = 1$  and  $J = 0.4$  as a function of the next-nearest neighbor interaction  $U_2$ .

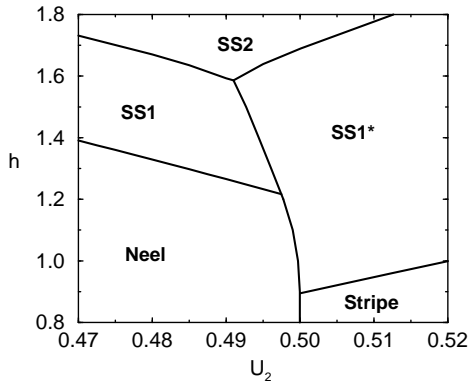


FIG. 18. The same as Fig. 17 but zoomed. The SS1\* phase is stable for slightly smaller values than  $U_2 = 0.5$ , which marks the transition between the Néel and the stripe phase.

In investigating the critical and multicritical behavior in the various parameter regions of the hard-core Bose-Hubbard model we have also found a rich variety of critical and multicritical phenomena.

*Superfluid to supersolid transition:* There are three different universality classes for the phase transition from the superfluid to the supersolid phases. These are the XSS-SF, CSS-SF and MSS-SF universality class for the transition from the superfluid (SF) to the checkerboard supersolid (SS1), stripe domain supersolid (SS1\*) and supersolid with an intermediate boson density profile (SS2). The CSS-SF transition is in the universality classes of the  $D = 2 + 1 = 3$  dimensional XY model. The critical fluctuations do not lead to deviations from Bose-liquid behavior at the transition. The critical phenomena at the XSS-SF transition are more interesting since it can either be fluctuation driven first order or be governed by a strong coupling fixed point implying that the superfluid component displays “non Bose-liquid” behavior. For phase diagrams of type I topology the phase transition from the superfluid to the mixed supersolid phase is always first order. Starting with  $U_2 \approx U_1/2$  (type II topology) one finds that within mean-field theory part of this phase boundary becomes second order and a tricritical point appears. The critical behavior at the second order line constitutes a new MSS-SF universality class, which is interesting in several respects. First of all, the trilinear coupling between the checkerboard and stripe domain order parameter induces criticality even for a massive checkerboard field at the phase boundary where the mass of the stripe domain field becomes zero. Second, the critical exponent for the “slaved” checkerboard field  $\phi$  are anomalously large already at the mean-field level. For instance one finds  $\phi_{\text{mf}} \propto \langle \psi \rangle^2$ , which implies  $\beta_{\phi}^{\text{mf}} = 1$ . We suppose that a detailed analysis [20] of this new universality class will reveal interesting critical anomalies; in particular there will be cusp-like singularities in the “slaved” checkerboard field.

*Supersolid to supersolid transition:* The phase transitions between the various supersolid phases can either be first or second order. If they are second order, they all belong to the XSS-SF universality class. In the parameter range where the checkerboard solid is the ground state at half-filling (type I topology) there is a first order transition from the checkerboard supersolid (SS1) to the mixed supersolid phase (SS2) at large fields (fillings). Lowering the field the transition becomes continuous at the tip of the SS2 phase. The critical behavior at this point is described by a new quantum tricritical model different from the  $D = 3$  classical Ising model. In the parameter range where the stripe domain solid is the ground state at half-filling there is no direct second order transition from the stripe domain supersolid (SS1\*) to the mixed supersolid (SS2); it is always first order. At certain regions of parameter space, however, there is an intermediate supersolid phase (SS3) and the first order line splits into two second order phase boundaries (both are in the XSS-SF universality class). At the tip of the intermediate SS3



phase there is a new bicritical quantum model. The effective action contains two Ising fields which are coupled by an anisotropic trilinear vertex. The structure of the effective action shows some resemblance with anisotropic Potts models.

*Supersolid to commensurate solid transition:* The phase transitions from the supersolid to the neighboring commensurate solid phases are all most likely mean-field like with logarithmic corrections in  $D = 2+1$  dimensions.

*Multicritical points:* For finite values of the hopping matrix element we have found up to seven different multicritical points on a single phase diagram. Some of them are novel type of quantum multicritical points. In particular, we found a new quantum tricritical point at the tip of the mixed supersolid phase. In the vicinity of these tricritical points there are critical end points with critical properties which are an interesting field for future investigations. Especially the critical end point with a critical “spectator phase” might engender novel “non Bose-liquid” behavior in the spectating phase.

**Acknowledgment:** It is a pleasure to acknowledge helpful discussions with Leon Balents, Markus Hummel, Uwe Täuber and Peter Young. This work was supported by the Deutsche Forschungsgemeinschaft (DFG) under Contract No. FR 850/2 and No. PI 337/1-1.

## APPENDIX A: SPIN-WAVE ANALYSIS OF THE 3/4 PHASE

In this section we present the main results of the spin-wave analysis of the 3/4 phase. Due to the four-sublattice structure we introduce four different Boson creation and annihilation operators  $(a_l^\dagger, a_l), (b_l^\dagger, b_l), (c_l^\dagger, c_l), (d_l^\dagger, d_l)$ . By using the linearized Holstein-Primakoff transformation for the first three with spin up ( $l \in \mathcal{L}_1, \mathcal{L}_2$  and  $\mathcal{L}_3$ ) and the fourth spin down ( $m \in \mathcal{L}_4$ ),

$$S_l^z = S - a_l^\dagger a_l \quad (\text{A1a})$$

$$S_l^x = \sqrt{\frac{S}{2}} (a_l + a_l^\dagger) \quad (\text{A1b})$$

$$S_l^y = -i\sqrt{\frac{S}{2}} (a_l - a_l^\dagger) \quad (\text{A1c})$$

$$S_m^z = -S + d_l^\dagger d_l \quad (\text{A1d})$$

$$S_m^x = \sqrt{\frac{S}{2}} (d_l + d_l^\dagger) \quad (\text{A1e})$$

$$S_m^y = -i\sqrt{\frac{S}{2}} (d_l - d_l^\dagger), \quad (\text{A1f})$$

and inserting in the Hamiltonian (Eq. 1.2) we derive the following Hamiltonian:

$$\mathcal{H} = -\frac{NSh}{2}$$

$$\begin{aligned} & + \sum_q \left[ A^{(1)} a_q^\dagger a_q + A^{(2)} b_q^\dagger b_q \right. \\ & + A^{(1)} c_q^\dagger c_q + A^{(4)} d_q^\dagger d_q \\ & + B_q (a_q b_q^\dagger + a_q^\dagger b_q + c_q d_{-q} + c_q^\dagger d_{-q}^\dagger) \\ & \left. + C_q (a_q d_{-q} + a_q^\dagger d_{-q}^\dagger + b_q c_q^\dagger + b_q^\dagger c_q) \right] \quad (\text{A2}) \end{aligned}$$

with the coefficients

$$A^{(1)} = h - 8SU_2 \quad (\text{A3a})$$

$$A^{(2)} = h + 8S(U_2 - U_1) \quad (\text{A3b})$$

$$A^{(4)} = -h + 8S(U_1 + U_2) \quad (\text{A3c})$$

$$B_q = -4SJ \cos q_x \quad (\text{A3d})$$

$$C_q = -4SJ \cos q_y. \quad (\text{A3e})$$

This bilinear Hamiltonian can be diagonalized by standard method, e.g. by introducing proper Greens functions. The excitation spectrum is then given by the zero of the following determinant

$$\begin{pmatrix} A^{(1)} - \omega & B_q & C_q & 0 \\ B_q & A^{(2)} - \omega & 0 & C_q \\ C_q & 0 & A^{(4)} + \omega & B_q \\ 0 & C_q & B_q & A^{(3)} - \omega \end{pmatrix} \quad (\text{A4})$$

As a result, we get a polynomial of fourth order in the excitation energy

$$\omega^4 + r\omega^3 + s\omega^2 + t\omega + u = 0 \quad (\text{A5})$$

with coefficients

$$r = A^{(4)} - A^{(2)} - 2A^{(1)} \quad (\text{A6a})$$

$$s = A^{(1)2} + 2A^{(1)}A^{(2)} - 2A^{(1)}A^{(4)} - A^{(2)}A^{(4)} \quad (\text{A6b})$$

$$\begin{aligned} t = & 2A^{(1)}A^{(2)}A^{(4)} + A^{(1)2}(A^{(4)} - A^{(2)}) \\ & - (B_q^2 - C_q^2)(A^{(2)} + A^{(4)}) \end{aligned} \quad (\text{A6c})$$

$$\begin{aligned} u = & -A^{(1)2}A^{(2)}A^{(4)} + A^{(1)}(A^{(2)} + A^{(4)})(B_q^2 + C_q^2) \\ & - (B_q^2 - C_q^2)^2. \end{aligned} \quad (\text{A6d})$$

This polynomial defines the four branches of the excitation spectrum. Calculating the soft-mode at  $q = 0$  leads to the phase boundaries of the 3/4 phase. Due to  $C_0 = B_0$  the spectrum can be simplified: the first solution is  $\omega = A^{(1)}$ , independent of  $q$ . The other solutions are given by a third order polynomial given by Eq. 2.23. For  $J = 0$  the solution are given by  $A^{(1)}, A^{(2)}$  and  $A^{(4)}$  from which the boundaries can be readily seen.

## APPENDIX B: SPIN-WAVE ANALYSIS OF THE SS1 AND SS1\* PHASE

These phases have two-sublattice spin structure which can be characterized by the wave vectors  $\tilde{q}$  which is  $q_0$  for

the SS1 phase and  $q_1$  and  $q_2$  for the SS1\* phase. Spin-wave calculation is done via the linearized transformation in Fourier space (Eq. 1.6c). The biquadratic term in the Bose operators can be written in the form [24]

$$\begin{aligned} \hat{H}^{(2)} = \sum_q & \left[ A_q a_q^\dagger a_q + \frac{B_q}{2} (a_q a_{-q} + a_q^\dagger a_{-q}^\dagger) \right. \\ & + C_q (a_q a_{-q-\tilde{q}} + a_q^\dagger a_{-q-\tilde{q}}^\dagger) \\ & \left. + D_q (a_q^\dagger a_{q+\tilde{q}} + a_{q+\tilde{q}}^\dagger a_q) \right] \end{aligned} \quad (\text{B1})$$

with coefficients

$$\begin{aligned} A_q = S & \left[ 2J_0 - U_q - J_q \right. \\ & + (2J_{\tilde{q}} + 2J_0 - 2U_{\tilde{q}} - 2U_0 \\ & - U_{q+\tilde{q}} - U_q + J_{q+\tilde{q}} + J_q) \sin^2 \gamma \sin^2 \delta \\ & + (2U_{\tilde{q}} - J_{q+\tilde{q}} - 2J_0 + U_q) \sin^2 \delta \\ & \left. + (2U_0 - 2J_0 - J_q + U_q) \sin^2 \gamma \right] \\ & + h \sin \gamma \cos \delta \end{aligned} \quad (\text{B2a})$$

$$\begin{aligned} B_q = S & \left[ U_q - J_q \right. \\ & + (U_q + U_{q+\tilde{q}} - J_q - J_{q+q_0}) \sin^2 \gamma \sin^2 \delta \\ & \left. + (J_{q+\tilde{q}} - U_q) \sin^2 \delta + (J_q - U_q) \sin^2 \gamma \right] \end{aligned}$$

$$C_q = S (J_q - U_q) \cos \gamma \sin \delta \sin \gamma \cos \delta \quad (\text{B2b})$$

$$\begin{aligned} D_q = S & \left[ (U_{\tilde{q}} + U_0 - J_{\tilde{q}} - J_0 + U_q - J_q) \right. \\ & \left. \times \cos \gamma \sin \delta \sin \gamma \cos \delta \right] \\ & + \frac{h}{2} \cos \gamma \sin \delta. \end{aligned} \quad (\text{B2c})$$

Here the angles  $\delta$  and  $\gamma$  are the difference and sum angles of the spins in respect to the magnetic field (Eq. 2.30 and Eq. 2.41). The excitation spectrum for this Hamiltonian then yields

$$E_q^{(i)} = \sqrt{(\Omega_1 \pm \Omega_2)/2}, \quad (\text{B3})$$

with

$$\begin{aligned} \Omega_1 = & A_q^2 - B_q^2 + A_{q+\tilde{q}}^2 - B_{q+\tilde{q}}^2 \\ & - 2(C_q + C_{q+\tilde{q}})^2 + 2(D_q + D_{q+\tilde{q}})^2, \\ \Omega_2^2 = & (A_q^2 - B_q^2 - A_{q+\tilde{q}}^2 + B_{q+\tilde{q}}^2)^2 \\ & + 4(D_q + D_{q+\tilde{q}}) \left[ (A_q + A_{q+\tilde{q}})^2 - B_q^2 - B_{q+\tilde{q}}^2 \right] \\ & - 4(C_q + C_{q+\tilde{q}}) \left[ (A_q - A_{q+\tilde{q}})^2 - B_q^2 - B_{q+\tilde{q}}^2 \right] \\ & + 8 \left\{ B_{q+\tilde{q}} B_q \left[ (D_q + D_{q+\tilde{q}})^2 + (C_q + C_{q+\tilde{q}})^2 \right] \right. \\ & \left. - 2(C_q + C_{q+\tilde{q}})(D_q + D_{q+\tilde{q}}) \right. \\ & \left. \times (A_q B_{q+\tilde{q}} + A_{q+\tilde{q}} B_q) \right\}. \end{aligned}$$

For the SS1 phase,  $\tilde{q} = q_0$ , a soft-mode appears at  $q_1$  and  $q_2$ . The spectrum for this wave vector can be simplified and vanishing of the second branch,  $E_q^{(2)}$ , leads to the condition

$$A_{q_1} - B_{q_1} - 2(D_{q_1} - C_{q_1}) = 0, \quad (\text{B5})$$

which defines with help of the angles  $\gamma$  and  $\delta$  a cubic equation in the field  $h$ . The tip of the SS2 lobe then is given by that point where two solutions are degenerated, i.e. where the discriminant vanishes.

In the striped phase SS1\*,  $\tilde{q} = q_1, q_2$ , there is a soft-mode at the checkerboard wave vector  $q = q_0$ . In this case the spectrum becomes a quartic function in the field and the tip of the SS2 lobe can be found by studying the corresponding cubic resolvent.

- 
- [1] A. Andreev and I. Lifshitz, Sov. Phys. JETP **29**, 1107 (1969).
  - [2] G. Chester, Phys. Rev. A **2**, 256 (1970).
  - [3] A. Leggett, Phys. Rev. Lett. **25**, 1543 (1970).
  - [4] A. Andreev, in *Quantum Crystals*, Vol. VIII of *Progress in Low Temperature Physics*, edited by D. Brewer (North Holland, Amsterdam, 1982), p. 68.
  - [5] H. Matsuda and T. Tsuneto, Suppl. Prog. Theor. Phys. **46**, 411 (1970).
  - [6] K. Liu and M. Fisher, J. Low. Temp. Phys. **10**, 655 (1973).
  - [7] G. Lengua and J. Goodkind, J. Low Temp. Phys. **79**, 251 (1990).
  - [8] M. Meisel, Physica B **178**, 121 (1992).
  - [9] C. Bruder, R. Fazio, and G. Schön, Phys. Rev. B **47**, 342 (1993).
  - [10] E. Roddick and D. Stroud, Phys. Rev. B **48**, 16600 (1993).
  - [11] A. van Otterlo and K.-H. Wagenblast, Phys. Rev. Lett. **72**, 3598 (1994).
  - [12] R. Scalettar, G. Batrouni, A. Kampf, and G. Zimanyi, Phys. Rev. B **51**, 8467 (1995).
  - [13] G. Batrouni, R. Scalettar, G. Zimanyi, and A. Kampf, Phys. Rev. Lett. **74**, 2527 (1995).
  - [14] A. van Otterlo *et al.*, Phys. Rev. B **52**, 16176 (1995).
  - [15] G. Murthy, D. Arovas, and A. Auerbach, Phys. Rev. B **55**, 3104 (1997).
  - [16] M. Fisher and P. Upton, Phys. Rev. Lett. **65**, 2402 (1990).
  - [17] M. Fisher and M. Barbosa, Phys. Rev. B **43**, 11 177 (1991).
  - [18] E. Frey and L. Balents, Phys. Rev. B **55**, 1050 (1997).
  - [19] Note, however, that the stability of the free energy requires constraints on the parameters  $u$  and  $v$ . Furthermore, in examining the flow diagram of the cubic model within  $\epsilon$ -expansion one finds that there are two regions in the  $(u, v)$ -plane which lie outside the domain of attraction of the stable fixed point (for a full discussion see

e.g. Ref. [25–27]). Adding a quadratic symmetry breaking term,  $g\psi_1\psi_2$ , even the first order transition (associated with the parameter regions of the  $(u, v)$ -plane which lie outside the domain of attraction of the stable fixed point) can become continuous. The phase diagram turns out to be rather complex with various interesting multicritical points [28].

[20] E. Frey and C. Pich (unpublished).

[21] M. Fisher, P. Weichman, and G. Grinstein, Phys. Rev. B **40**, 546 (1989).

[22] If one introduces new fields  $\sigma = \psi_1 + \psi_2$  and  $\pi = \psi_1 - \psi_2$  one obtains an effective action with a uniaxial anisotropy (induced by the quadratic symmetry breaking field  $g$ ) and a cubic symmetry breaking field  $\tilde{v}$ . Then the effective action discussed here closely resembles the structure of a free energy discussed Bruce and Aharony [29] in the context of classical critical phenomena. They find that for number of spin components  $n < n_c(D)$ , where  $n_c(D)$  is the critical number of components above which the cubic

fixed point becomes stable, the critical lines separating the intermediate phase from the other two phases merge into a single “flop” line making the tetracritical point apparently bicritical. Similar conclusion should hold here but differences could result due to the coupling to the superfluid phase.

[23] A. Theumann and W. Theumann, Phys. Rev. B **26**, 3856 (1982).

[24] C. Pich, Ph.D. thesis, Technische Universität München, 1994.

[25] T. Nattermann and S. Trimper, J. Phys. A **8**, 2000 (1975).

[26] I. Lyuksyutov and V. Prokrovskii, JETP Lett. **21**, 9 (1975).

[27] I. Lyuksyutov, Phys. Lett. **56A**, 135 (1976).

[28] M. Kerszberg and D. Mukamel, Phys. Rev. B. **23**, 3943 (1981).

[29] A. Bruce and A. Aharony, Phys. Rev. B **11**, 478 (1975).